

Dynamics of interactions of antiprotons and antinuclei with nuclei in Geant4

A.S. Galoyan*

VBLHEP, JINR

E-mail: galoyan@lxpub01.jinr.ru

A. Ribon

CERN, Geneva

E-mail: Alberto.Ribon@cern.ch

V.V. Uzhinsky

LIT, JINR

E-mail: uzhinsky@jinr.ru

On behalf of the Geant4 Collaboration

Antiproton-proton, antiproton-nucleus and antinucleus-nucleus interactions are considered in Dual-Parton or Quark-Gluon-String model. The model assumes creation and fragmentation of quark-gluon strings in the interactions. Cross sections of various processes of the creation are determined by an analysis of experimental data on antiproton-proton interactions. Geant4 LUND fragmentation model is used for the simulation of the string fragmentations. As a result, a good description of a wide set of experimental data is reached.

A generalization of the approach for antiproton-nucleus and antinucleus-nucleus interactions requires a knowledge of total and inelastic cross sections of these processes. The cross sections are calculated in the Glauber approximation. Good results are obtained for all experimentally known cross sections.

Usually, the asymptotic Abramovsky-Gribov-Kancheli (AGK) cutting rules are applied for a determination of the multiplicity of produced strings. We propose finite energy corrections to the AGK rules for an extension of the model to low energy domain. Using the cutting rules and the corrections, we describe antiproton-nucleus interactions starting from low energies ($E > 50$ MeV) up to 1000 GeV. We also reproduce known experimental data on antideuteron interactions with nuclei.

So, we have created a unified model of antiproton-proton, antiproton-nucleus and light antinucleus-nucleus interactions. The model reproduces general properties of the interactions. The model is implemented in the FTF model of Geant4 toolkit and can be accessed using the FTF_BERT PhysicsList.

XXII International Baldin Seminar on High Energy Physics Problems

15-20 September, 2014

JINR, Dubna, Russia

*Speaker.

Introduction

Recently, a new interest to antibaryon and antinucleus interactions with nuclei has been arisen. It is connected with results obtained at RHIC and LHC accelerators, especially, with observations of helium antinuclei in nucleus-nucleus interactions at super high energies. STAR and ALICE collaborations have found antihelium nuclei. The number of observed antinuclei is very small, but it is only beginning. There is also cosmic space experiments like PAMELA, BESS, AMS, CAPRISE and so on which are going to search antinuclei in cosmic rays. They hope this will bring a new light on the question about antimatter in our Universe. A detailed experimental study of antiproton-proton and antiproton-nucleus interactions is foreseen at the future FAIR facilities (GSI, Darmstadt, Germany) by the PANDA Collaboration. The accelerator experiments and the cosmic ray experiments need estimations of properties of antiproton and antinuclei interactions ($\bar{p}A, \bar{A}A$) with nuclei for reconstruction and identification of antinuclei and reaction products. This requires a code for a good simulation of $\bar{p}A$ and $\bar{A}A$ interactions. Recently, it becomes possible to simulate the interactions in the well-known Geant4 toolkit [1]. At the creation of the simulation code, we used main assumptions of the Dual-Parton or Quark-Gluon-String model (DPM/QGSM) [2] and Glauber approach [3, 4, 5].

In Fig. 1 we present quark flow diagrams of processes considered usually in DPM:

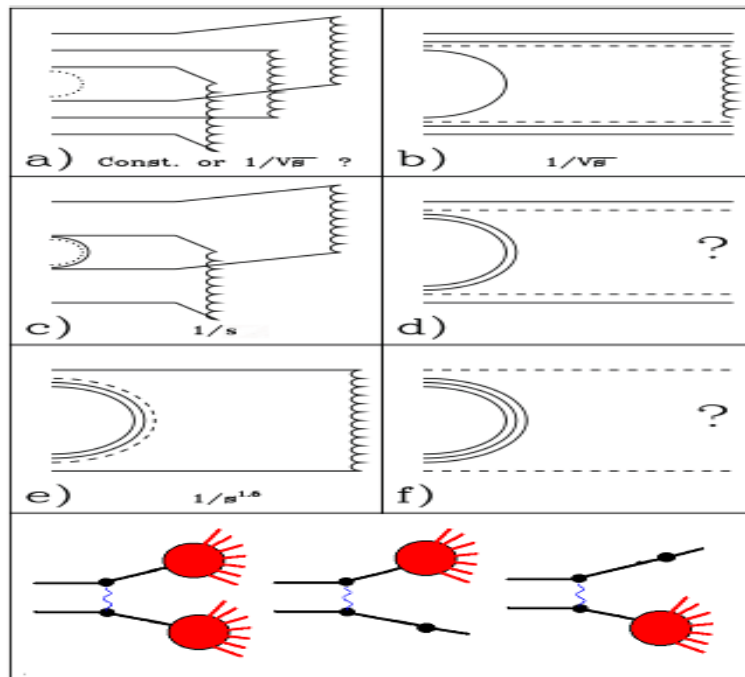


Figure 1: Quark flow diagrams of $\bar{p}p$ interactions.

The diagram "a" corresponds to string junction's annihilation with 3 quark-antiquark string's creation. The string junction is a gluonic object which couples together quarks in baryon. The diagram "b" represents quark and antiquark annihilation leading to diquark-antidiquark string creation. The diagram "c" corresponds to quark-antiquark and string junction's annihilations with creation of 2

quark-antiquark strings. Diagrams "d" and "f" can be responsible for exotic meson production. The last diagrams at the bottom of the figure are important at high energies. They are connected with pomeron exchange in t-channel.

Energy dependencies of the cross sections of the processes in some cases are predicted by the reggeon phenomenology. They are also shown in the figure. An elaborated scheme for a calculation of the cross sections in the phenomenology was proposed in our papers [6, 7]. As was shown in the papers, the approach is valid at $P_{lab} > 3 \text{ GeV}/c$. Because experimental studies require much less energies, we undertook a new attempt to estimate the cross sections. It is presented in the next section.

1. Estimation of the process cross sections

Let us start with the simplest process "b" – diquark-antidiquark string creation. This process leads to baryon-antibaryon production in the final state (for example, neutron-antineutron – $\bar{n}n$, lambda-antilambda – $\bar{\Lambda}\Lambda$, and so on). $\bar{n}n$ state can be produced at a single breakup of the string. Thus, the cross section of the process, $\sigma_{\bar{n}n}$, can be expressed as a product of the cross-section of process "b" (σ_b) and a probability of two particles decay of the string (P_2):

$$\sigma_{\bar{n}n} = \sigma_b \cdot P_2(M = \sqrt{s})$$

. Because below meson production threshold $P_2 = 1$, this expression allows to estimate σ_b . The corresponding experimental data can be parameterized as

$$\sigma_b = \sigma_{\bar{n}n} \simeq 15.65 + 700 \cdot (M_{th} - \sqrt{s})^{2.5} \quad (mb) \quad \sqrt{s} \leq M_{th}, \quad M_{th} = 2.172 \text{ GeV}.$$

At higher energies according to the reggeon phenomenology, σ_b must decrease as C/\sqrt{s} . Experimental value of $\sigma_{\bar{n}n}$ at the threshold allows one to find that $C = 34 \text{ (mb GeV)}$. Choosing P_2 in the simplest exponential form, $P_2 = \exp[-B(M - M_{th})]$, we determine B which fit $\sigma_{\bar{n}n}$, $B = 0.5 \text{ (GeV}^{-1}\text{)}$. Implementing this function in the LUND string fragmentation model we describe (see Fig. 2a) other reactions with baryon and antibaryon in the final states ($\bar{\Lambda}\Lambda$, $\bar{\Lambda}\pi^0\Lambda$, $\bar{\Lambda}\pi^+\pi^-\Lambda$).

The other simple process is a creation of a single quark-antiquark string (process "e"). It can be responsible for productions of 2, 3 and 4 mesons. For example, cross sections of the reactions: $\bar{p}p \rightarrow \pi^+\pi^-$ and $\bar{p}p \rightarrow \pi^+\pi^-\pi^0$, can be given by the following expressions:

$$\begin{aligned} \sigma_{\pi^+\pi^-} &= \sigma_e \cdot P_2(M = \sqrt{s}) \\ \sigma_{\pi^+\pi^-\pi^0} &= \sigma_e \cdot [1 - P_2(M = \sqrt{s})] \int P_F(\sqrt{s}, M) P_2(M) dM, \end{aligned}$$

where P_F is a single step fragmentation function. The expressions contain σ_e and P_2 . For determination of the last function¹, we used a ratio of experimental $\sigma_{\pi^+\pi^-\pi^0}$ and $\sigma_{\pi^+\pi^-}$ and found

$$P_2 \simeq \exp[-B(M^2 - M_{th}^2)], \quad B = 0.88 \text{ (GeV}^{-2}\text{)}, \quad M_{th} = 0.38 \text{ (GeV)}.$$

For description of the experimental data, we set $\sigma_e = 140/s \text{ (mb)}$. With all of these, we describe the data on 2 meson's production in $\bar{p}p$ interactions (see Fig. 2b) quite well.

¹Neglecting a contribution of the process "c".

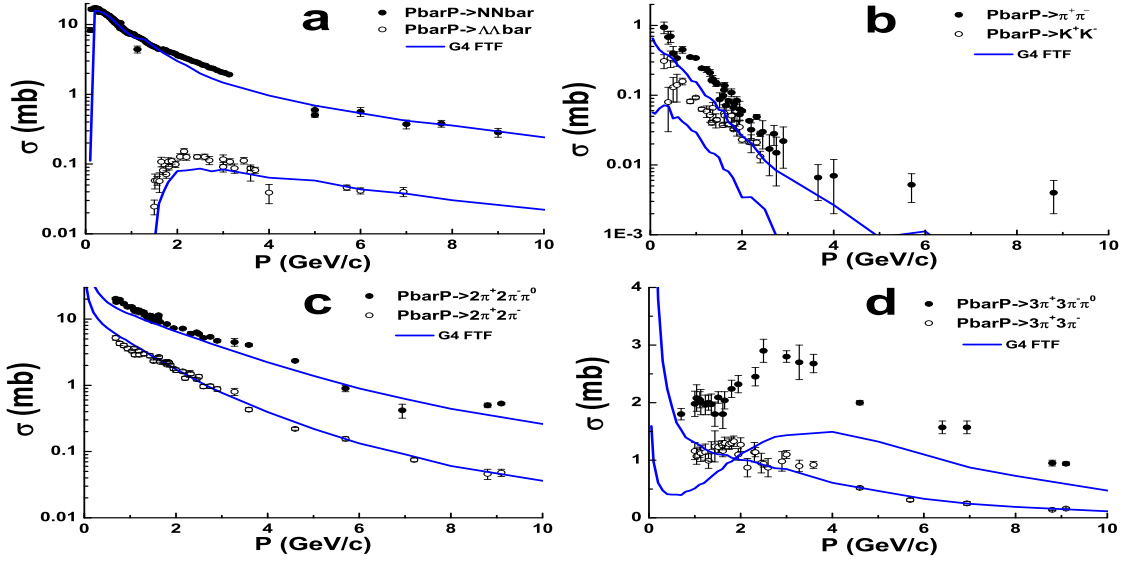


Figure 2: Channel cross sections of $\bar{p}p$ interactions. Points are experimental data gathered in [8]. Lines are our calculations.

Having known quark-antiquark string fragmentation, we can estimate cross section of process "a" (creation of 3 quark-antiquark strings). Using σ_a in a form $25/\sqrt{s-4m^2}$ (mb), we calculated cross-sections of processes $\bar{p}p \rightarrow 2\pi^+2\pi^-$, $\bar{p}p \rightarrow 2\pi^+2\pi^-\pi^0$, $\bar{p}p \rightarrow 3\pi^+3\pi^-$ and $\bar{p}p \rightarrow 3\pi^+3\pi^-\pi^0$ (Fig. 2c, 2d).

Sum of the cross sections of the processes "a", "b" and "e" is below $\bar{p}p$ inelastic cross section at $P_{lab} \leq 700$ MeV/c. We ascribe the deficit to the cross section of the process "c", $\sigma_c = \sigma_{\bar{p}p}^{in} - \sigma_a - \sigma_b - \sigma_e$, and parameterize it as $\sigma_c = 40 \cdot m^2/s\sqrt{s-4m^2}$ (mb).

Processes without annihilations dominate at high energies. They are presented in the bottom of Fig. 1. Their cross sections can be described by $\sigma_{FTF} = 35 \cdot (1 - 2.1/\sqrt{s})$ (mb). We use for simulations of the processes FTF model of Geant4 [9].

The estimated cross sections, the improved string fragmentation algorithm and the FTF model of Geant4 allow to describe general properties of $\bar{p}p$ interactions, especially channel cross sections presented in Fig. 2. Thus, we conclude the existing phenomenology of antibaryon-baryon annihilation and hadron-nucleon high energy interactions with corresponding cross sections can be considered as a unified base for understanding of the $\bar{p}p$ interactions.

2. Cross sections of $\bar{p}A$ and $\bar{A}A$ interactions

It is natural to use the Glauber approach for calculations of the cross sections. For the first time a good description of elastic antiproton-deuteron scattering was reached in the classical paper by V. Franco and R.J. Glauber [10] in 1966. After that, in 1985 O.D. Dalkarov and V.A. Karmanov [11] showed that elastic and inelastic (with excitation of nuclear levels) antiproton scattering on C, Ca, and Pb nuclei are described quite well at \bar{p} kinetic energies of 46.8 and 179.7 MeV within the approximation. The Glauber approach in the question was also used in many other papers.

The elastic scattering amplitude of an antinucleus containing \bar{A} antibaryons on a target nucleus with mass number A is given as [4]:

$$F_{\bar{A}A}(\vec{q}) = \frac{i}{2\pi} \int d^2b e^{i\vec{q}\vec{b}} \left\{ 1 - \prod_{i=1}^{\bar{A}} \prod_{j=1}^A \left[1 - \gamma(\vec{b} + \vec{\tau}_i - \vec{s}_j) \right] \right\} |\Psi_{\bar{A}}|^2 |\Psi_A|^2. \quad (2.1)$$

$$\left(\prod_{i=1}^{\bar{A}} d^3 t_i \right) \left(\prod_{j=1}^A d^3 r_j \right) = i \int_0^\infty b P_{\bar{A}A}(b) J_0(qb) db,$$

where the same nomenclature as in [4, 11] is used, in particular γ is the amplitude of an elastic antinucleon-nucleon scattering in the impact parameter representation averaged over the spin and isospin degrees of freedom,

$$\gamma(\vec{b}) = \frac{1}{2\pi i} \int d^2q e^{i\vec{q}\vec{b}} F_{\bar{N}N}(\vec{q}).$$

The amplitudes are normalized so that a differential elastic scattering cross section can be written as: $d^2\sigma/dq^2 = |F(\vec{q})|^2$, where \vec{q} is the momentum transfer ($t = -\vec{q}^2$). The corresponding total cross section is $\sigma_{\bar{A}A}^{tot} = 4\pi \text{Im}F(0)$.

Quite often γ is parameterized as:

$$\gamma(\vec{b}) = \frac{\sigma_{\bar{N}N}^{tot} (1 - i\rho)}{4\pi \beta} e^{-\vec{b}^2/2\beta},$$

where $\sigma_{\bar{N}N}^{tot}$ is the total cross section of the antinucleon-nucleon interactions, ρ is the ratio of the real to imaginary parts of the $\bar{N}N$ elastic scattering amplitude at zero momentum transfer, and β is the slope parameter of the $\bar{N}N$ differential elastic scattering cross section. Then

$$F_{\bar{N}N}(\vec{q}) = \frac{i}{4\pi} \sigma_{\bar{N}N}^{tot} (1 - i\rho) e^{-\beta\vec{q}^2/2},$$

where β is:

$$\beta = (\sigma_{\bar{N}N}^{tot})^2 (1 + |\rho|^2) / (16 \pi \sigma_{\bar{N}N}^{el} 0.3897).$$

Here, $\sigma_{\bar{N}N}^{el}$ is the $\bar{N}N$ elastic cross section and 0.3897 is a coefficient required in order to express β in units of $(GeV/c)^{-2}$, if the cross sections are given in millibarns. We have considered parameterizations of energy dependencies of total and elastic antinucleon-nucleon scatterings which are needed for calculations in our recent publication [12].

The squared modulus of the wave function is usually written as:

$$|\Psi_A|^2 = \delta\left(\sum_{i=1}^A \vec{r}_i/A\right) \prod_{i=1}^A (\rho_A(\vec{r}_i)/A).$$

ρ_A/A coincides with the one-particle density of the nucleus, if one neglects the center-of-mass correlation connected with the δ -function. The densities for heavy nuclei were chosen to have the standard Woods-Saxon distribution with the parameters given in [13]. The correlations were accounted for according to [14]. We use the gaussian parameterization for light (t , ${}^3\text{He}$, ${}^4\text{He}$) nuclei and for the corresponding antinuclei:

$$\rho_A(\vec{r}) = \frac{A}{(\pi R_A^2)^{3/2}} e^{-\vec{r}^2/R_A^2}, \quad R_{3H} = R_{3He} = 1.81 \text{ (fm)}, \quad R_{4He} = 1.37 \text{ (fm)}.$$

The squared modulus of the (anti) deuteron wave function was chosen as the sum of three gaussians [15].

Many approximations have been proposed in order to simplify the calculation of P_{hA} and P_{AB} . Most effective one is a method proposed in [16] in which the amplitude is found as an average over various samples of the nucleon coordinates:

$$P_{AB}(\vec{b}) \simeq \frac{1}{N} \sum_{\alpha=1}^N \left\{ 1 - \prod_{i=1}^A \prod_{j=1}^B \left[1 - \gamma(\vec{b} + \vec{r}_j^\alpha - \vec{s}_i^\alpha) \right] \right\}, \quad (2.2)$$

where N is the volume of the samples. The nucleon coordinates are sampled according to the measure $|\Psi_A|^2 |\Psi_B|^2$. The method consists of multiple sampling of the nucleon coordinates according to the function $|\Psi_A|^2 |\Psi_B|^2$, calculation of the expression in braces of Eq. 2.2 for each sampling, and an averaging of the calculation results over the samples. This method is implemented in the DIAGEN code [16]. Using it, one can calculate various cross sections of antiproton-nucleus and antinucleus-nucleus interactions – total, elastic, quasi-elastic and inelastic cross sections.

We show in Fig. 3 our calculations in comparison with experimental data. For projectile antideuterons we present experimental data [18] at two energies – 13.3 and 25 GeV/c (open and close circles, correspondingly) and calculation results at the energies (solid and dashed lines). As seen, the agreement between the experimental data and the calculations is rather good. More details of the calculations and results are reported in [12].

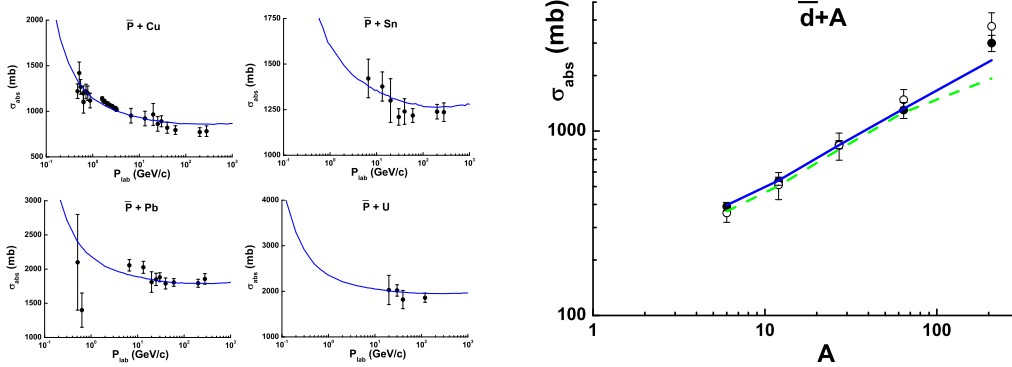


Figure 3: Absorption cross sections of antiproton and antideuteron interactions with nuclei. The points are experimental data [17, 18], the lines are our calculations.

3. Finite energy corrections to AGK cutting rules

It is known that a projectile has multiple intra-nuclear collision in a target at high energies, or involves some nuclear nucleons at the fast stage of interactions. Distribution on the multiplicity of the involved nucleon, ν , can be found applying the asymptotic Abramovsky-Gribov-Kancheli (AGK) cutting rules [19] to elastic scattering amplitude. The application of the rules to the elastic antiproton-nucleus scattering amplitude gives results:

$$\sigma_{\bar{p}A}^{prod} = \sigma_{\bar{p}A}^{tot} - \sigma_{\bar{p}A}^{el} - \sigma_{\bar{p}A}^{q.el} = \int d^2b \left\{ 1 - \left[1 - \frac{1}{A} \int g(\vec{b} - \vec{s}) \rho_A(\vec{s}, z) d^2s dz \right]^A \right\} = \sum_{\nu=1}^A \sigma_{\nu}, \quad (3.1)$$

$$\sigma_v = C_A^v \int d^2b \left[\frac{1}{A} \int g(\vec{b}-\vec{s}) \rho_A(\vec{s}, z) d^2s dz \right]^v \cdot \left[1 - \frac{1}{A} \int g(\vec{b}-\vec{s}) \rho_A(\vec{s}, z) d^2s dz \right]^{A-v}, \quad (3.2)$$

$$g(\vec{b}) = \gamma(\vec{b}) + \gamma^*(\vec{b}) - \gamma(\vec{b}) \cdot \gamma^*(\vec{b}).$$

As seen from the expression, v can be varied in a wide range at large A . But it obvious that at low energies a projectile can have only one inelastic collision in a nucleus. After the collision an intra-nuclear cascade of secondary particles takes place. Therefore, the AGK rules must be corrected at low energies. Here we use the following consideration² [20].

According to high energy phenomenology let us assume that a projectile hadron interacts with a target, if there are slow partons capable to interact in the projectile. Let an average life time of the slow parton fluctuation in the projectile rest frame is τ_0 . In the rest frame of the target, the time will be $\gamma \cdot \tau_0$, where γ is Lorentz factor of the projectile. During this time, the projectile flies a distance $l = v \cdot \gamma \cdot \tau_0 = (P_{lab}/m_p) \cdot \tau_0$. In a case of interaction with a nucleus, the projectile meets, at the average, $v_{max} = \sigma \rho_A \tau_0 \cdot (P_{lab}/m_p) = P_{lab}/P_0$ target nucleons. Here σ is a projectile-nucleon cross section, ρ_A is the average nuclear density $\sim 0.15 \text{ fm}^{-3}$, P_0 is a parameter. Because at $P_{lab} = 0$ there can be inelastic antiproton-proton interactions, we use in our calculation the integer part of P_{lab}/P_0 increased by one as v_{max} .

Let us introduce v_{max} in the expression for antiproton-nucleus production cross section,

$$\sigma_{\bar{p}A}^{prod} = \int d^2b \left\{ 1 - \left[1 - \frac{1}{A} \int g(\vec{b}-\vec{s}) \cdot \rho_A(\vec{s}, z) d^2s dz \right]^A \right\} =$$

$$\simeq \int d^2b \left\{ 1 - e^{-\int g(\vec{b}-\vec{s}) \cdot \rho_A(\vec{s}, z) d^2s dz} \right\} = \int d^2b \left\{ 1 - \left[e^{-\frac{1}{v_{max}} \int g(\vec{b}-\vec{s}) \cdot \rho_A(\vec{s}, z) d^2s dz} \right]^{v_{max}} \right\}$$

$$= \sum_{v=1}^{v_{max}} \sigma'_v,$$

$$\sigma'_v = C_{v_{max}}^v \int d^2b \left[1 - e^{-\frac{1}{v_{max}} \int g(\vec{b}-\vec{s}) \cdot \rho_A(\vec{s}, z) d^2s dz} \right]^v \cdot e^{-\frac{v_{max}-v}{v_{max}} \int g(\vec{b}-\vec{s}) \cdot \rho_A(\vec{s}, z) d^2s dz}. \quad (3.3)$$

As seen, a number of intra-nuclear collisions in the case cannot be large than v_{max} .

The same expression can be obtained, if one assumes that after each interaction predicted by Eq. 3.2 a probability of the next interaction is decreased by $1/v_{max}$. An algorithm implementing this interpretation looks like that: at the beginning, a projectile has a power, P , to interact with v_{max} nucleons ($P = v_{max}$). Thus a probability of an interaction with the first nucleon, P/v_{max} , is equal to 1. The power decreases after the interaction on 1. The probability of an interaction with the second nucleon is equal to P/v_{max} , where $P = v_{max} - 1$. If the second interaction is happened, the power is decreased once more. In other case, it is left on the same level. This is applied for each possible interaction.

As a result, we have that at low energies $v_{max} = 1$, thus a projectile can have only one interaction inside a target, and the usual cascading takes place. At higher energies, v_{max} will be larger, and two or more nucleons can be involved. Only these nucleons will participate in the interactions

²A complicated consideration of hadron-nucleus interactions in the reggeon phenomenology – consideration of yields of planar and non-planar, enhanced and semi-enhanced diagrams is not finished yet. Thus, we present simplified approach.

describing by the string models. Using hadron-nucleus experimental data, a tuning of only one parameter, P_0 , gives a value of $P_0 \sim 3\text{--}6$ GeV/c.

Usually, the formation time concept is introduced when considering a secondary particle cascading inside a nucleus. It is assumed that a particle created in a defined space-time position can interact with other nucleons only after formation time determined in the particle rest frame. But, real particles are not point-like objects. Therefore, the concept was criticized in the paper [21], where it was considered the particle cascading in the reggeon phenomenology. Another attempt was presented in the paper [22], where a simplified model was proposed – a reggeon theory inspired model (RTIM). We use the RTIM model in our calculations. More exactly, we use the above given algorithm for a sampling of a multiplicity of intra-nuclear collisions. After this, RTIM is applied. The next step is a simulation of particle production. We ascribe the formation time to each of the produced particles. All of these decrease the upper limit of the formation time application.

All calculations presented below are performed with the finite energy corrections.

4. Validation of the model for antiproton-nucleus and antinucleus-nucleus interactions

Understanding and explanation of inelastic antibaryon-nucleus interactions – multiplicities of produced mesons, protons and neutrons, distributions of the particles on kinematical variables and their dependencies on energy of the projectile and mass number of a target nucleus are very complicated tasks. In the first rough approximation, one can assume that an interaction of an antibaryon with a nuclear nucleon is identical to the interaction with a free nucleon neglecting the binding energy of the nucleon, ~ 10 MeV. So, the main effects have to be connected with secondary particles cascading within a nucleus. The existing intra-nuclear cascade models have passed a long history of development, and allow to simulate now meson and baryon interactions with nuclei satisfactorily. Two of such models are presented in Geant4 – the Bertini cascade model (BERT) and the binary cascade model (BIC) [23]. There is also a simplified model – the precompound model interface (PRECO), which only absorbs low energy particles ($E \leq 10$ MeV) produced by a high energy generator and located in a nuclear residual, and ascribes them to the residual nuclei. The binary model and the precompound model can be easily coupled with the FTF model. Therefore, we use in our following calculations two combinations of the models: FTF+BIC and FTF+PRECO³. FTFP demonstrates properties of interactions without intra-nuclear cascading. FTFB shows effects of the cascading.

The binary model simulates a propagation of particles in 3-dimension space of a nucleus viewed as a potential well with nucleons in it. All elementary interactions (meson-nucleon and baryon-nucleon) are considered as binary reactions with one (meson-nucleon) or two particles in a final state. A wide set of meson and baryon resonances are taken into account. The Pauli-blocking is applied to the final state – collisions and decays of resonances for which any secondary nucleon has a momentum, p_i , below the local Fermi momentum, i.e. $p_i < p_F^{max}(r)$, are suppressed.

Properties of a nuclear residual are calculated when all cascading particles are left the nucleus. De-excitation of the residual nucleus characterized by the number of nucleons in it, its

³These combinations are denoted as FTFB and FTFP, respectively.

charge, the number of holes, the number of all excitons, the number of charged excitons, and its four-momentum is simulated applying pre-equilibrium model and Generalized Evaporation Model (GEM) [24].

As shown in Fig. 4 and 5, FTFB describes the general properties of antiproton-nucleus interactions qualitatively. FTFP gives low yields of protons and neutrons. Thus, accounting of the particles cascading is very important for a correct simulation of the reactions.

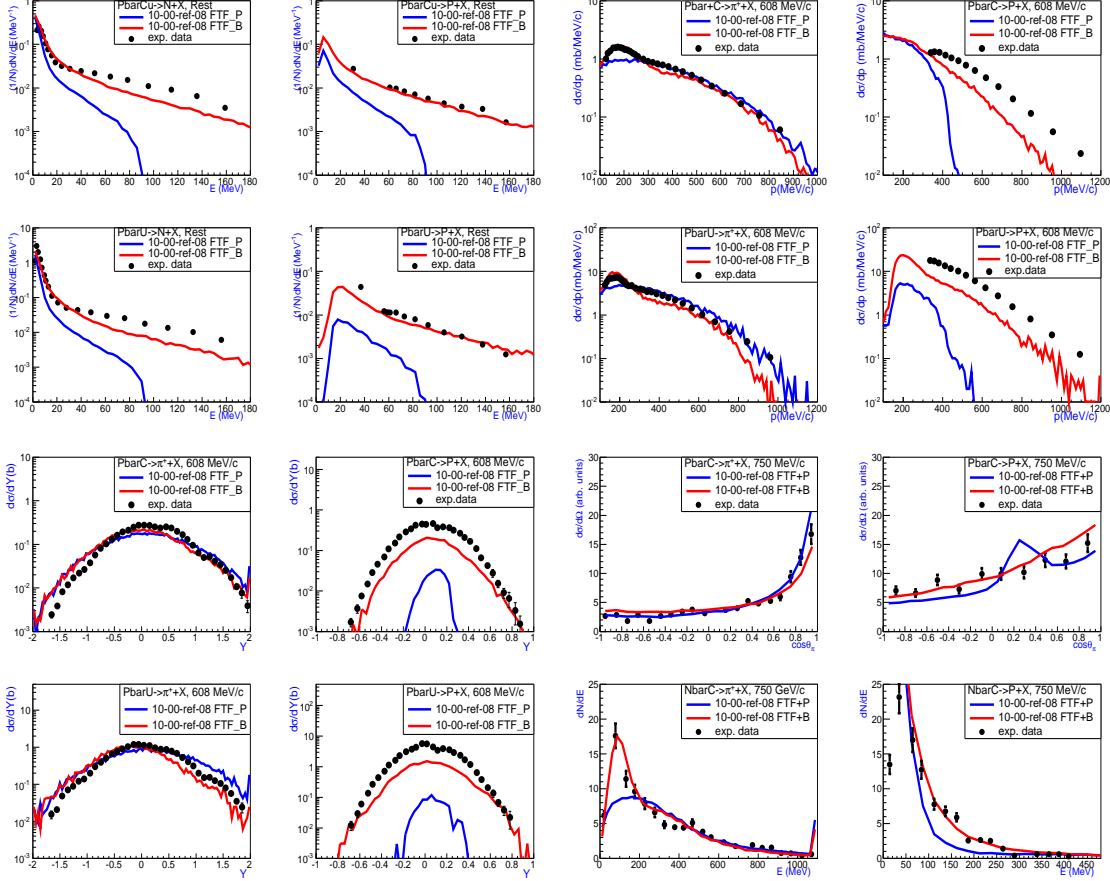


Figure 4: Protons, neutrons and π^+ mesons distributions on kinematical variables in antiproton-nucleus interactions at various energies. Points are experimental data [25]. Lines are our calculations. Red and blue lines are calculations with FTFB and FTFP, respectively.

As seen, FTFB reproduces evaporated neutron yield at $E_n \leq 30$ MeV. The yield of the pre-equilibrium nucleons, $E_n > 30$ MeV, is underestimated. It is typical for cascade models [26] at intermediate energies. An inclusion of a deep antibaryon potential in nuclei, ~ -150 MeV, can improve a situation with the description of the proton spectra [27]. π -meson spectra are described quite well.

Calculation results for higher energies are presented in Fig. 5. In upper figures, we show kinetic energy spectra of neutrons produced in \bar{p} interactions with Al and Cu at emission angles of 50 and 145 degree. As seen, the combination of the FTF model and the binary model gives results

which are in agreement with the experimental data for forward emitted neutrons at the angle of 50 degree. At the same time, the combination underestimates the production of neutrons emitted in backward hemisphere at the angle of 145 degree. FTF+PRECO calculations are below of the experimental data essentially.

Kinetic energy spectra of neutrons produced in \bar{p} interactions with heavy nuclei are plotted in the bottom figures. As seen, FTF+BIN works quite well for the data as well as for forward and backward emitted neutrons.

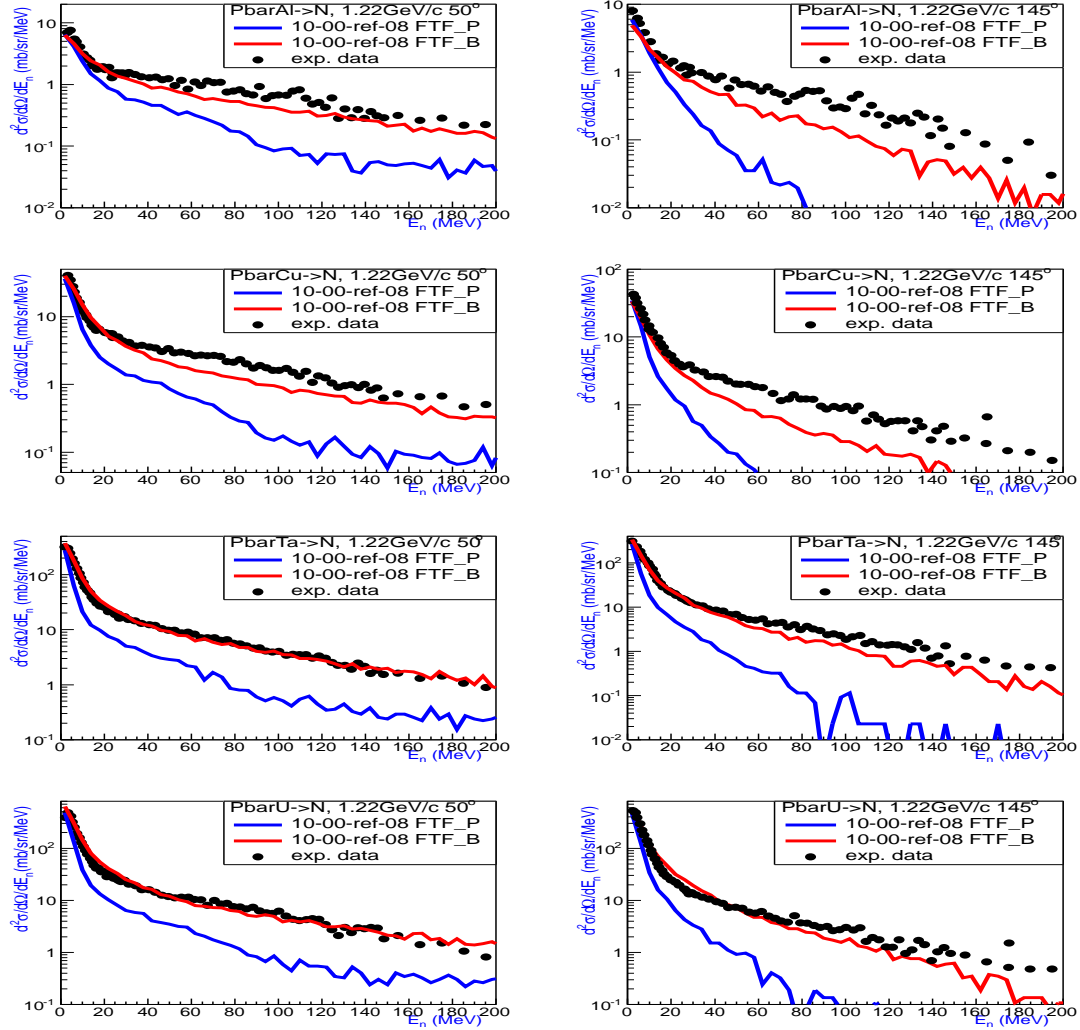


Figure 5: Neutron kinetic energy spectra in antiproton-nucleus interactions. Points are experimental data [28]. Lines are our calculations.

At high energies, a probability of the annihilation in $\bar{p}p$ interactions is small. Thus, the main processes in $\bar{p}A$ collisions are inelastic interactions of antiprotons with nuclear nucleons. Here, the FTF model works rather well as seen in Fig. 6. In the figure, we show Feynman X distributions of protons and antiprotons in p and \bar{p} interactions with Be, Cu, Ag, W and U at projectile momentum of 120 GeV/c. Points are experimental data from the paper [29]. Lines are our calculations by FTF

+ PRECO. As seen, there is a good agreement between the results and the data at $x_F > 0.15$ for projectile antiprotons, and $x_F > 0.2$ for projectile protons except Be target. The model reproduces the A-dependence of the spectra and the experimental suppression of the antiproton spectra with respect to protons. Nearly the same results were obtained in Ref. [29], where the data were analyzed on the base of DPM.

Two peculiarities are presented in our calculations – a peak at large values of x_F connected with quasi-elastic scattering of the projectile particles and the underestimation of the spectra at small x_F . The peak is absent in the data due to the experimental conditions. The underestimation is caused by insufficient antibaryon-baryon pair production in the central region of nucleon-nucleon collisions in the Fritiof (FTF) model. It is desirable to improve the description in the future.

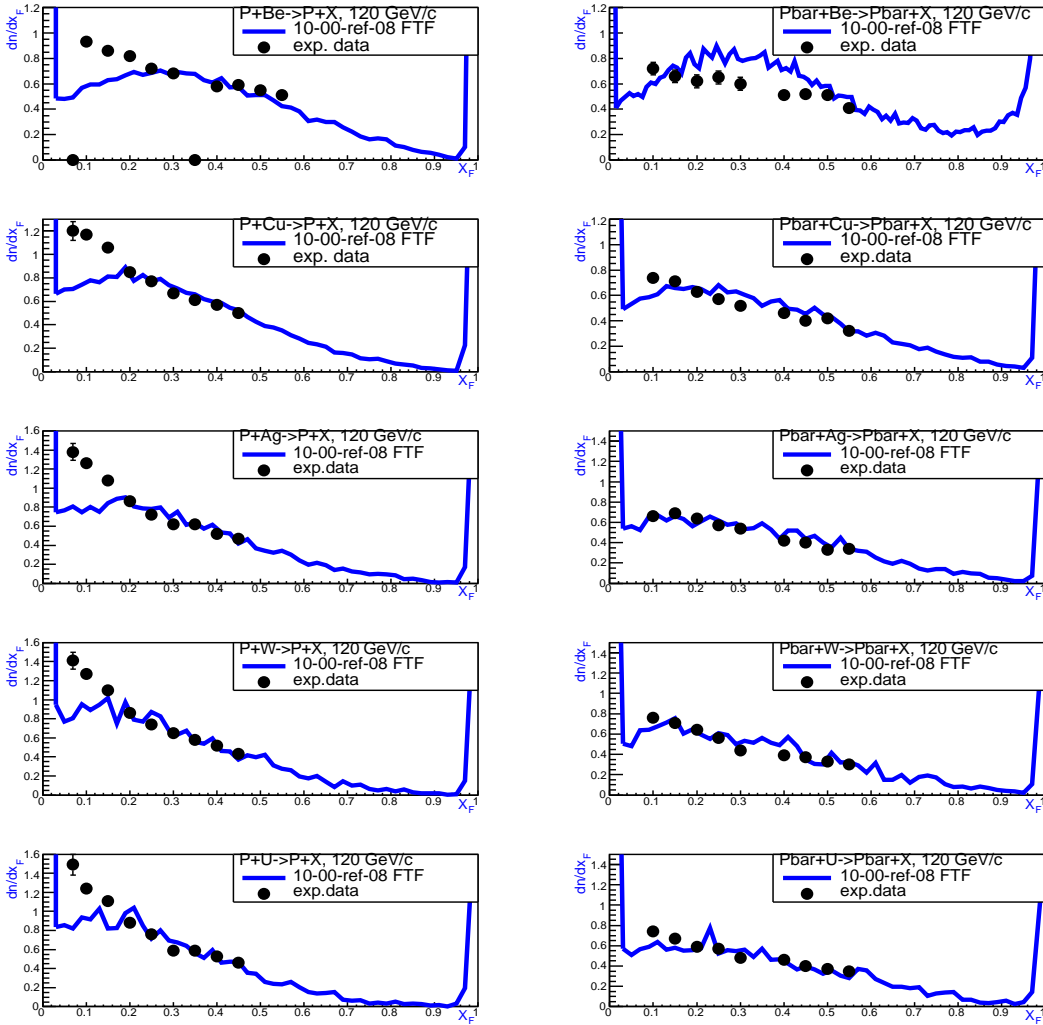


Figure 6: Protons and antiprotons x_F distributions in pA and $\bar{p}A$ interactions. Points are experimental data [29]. Lines are our calculations.

π -mesons are dominating among produced particles at high energies. Their multiplicities are mainly determined by the multiplicity of the intra-nuclear collisions which is calculated using

AGK cutting rules or Glauber approach. Many Monte Carlo models use the approach, and they are distinguished by details of the production mechanism, but they have a minor influence on the multiplicities. Probably, fine differences can be found in particle's distributions on kinematical variables. As shown in Fig. 7, the FTF model reproduces general properties of mesons produced in $\bar{p}A$ interactions. First of all, the model FTF describes A-dependence of the spectra in the central region. Calculation results are very close to the experimental data for π^- mesons. Insufficient yield of positive charged particles is observed in the model in the target fragmentation region. The result can be improved applying more elaborated model for the particle cascading. It would be well to check the correctness of the description of the proton production in the target fragmentation region. We believe that peaks presented in the data at $\eta \sim 0$ are connected with these protons. More detailed experimental data in the region are needed for a firm conclusion about the model quality.

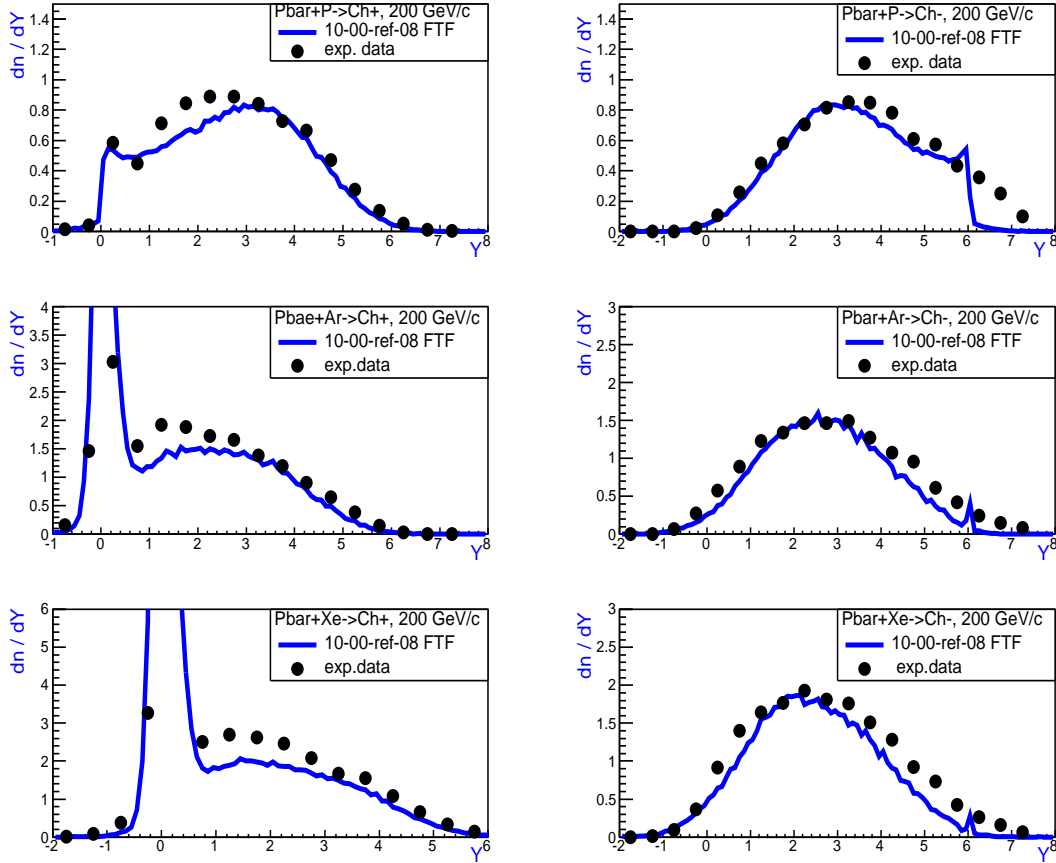


Figure 7: Pseudo-rapidity distributions of positive and negative charged particles in antiproton-nucleus interactions at 200 GeV/c. Points are experimental data [30]. Lines are our calculations.

Let us go to antinucleus-nucleus interactions. For these interactions, we have calculated cross sections using Glauber model and our parameterizations of total and elastic $\bar{p}p$ cross sections. For simulation of antinucleus-nucleus interactions in the FTF model, we also applied AGK rules with

the low energy corrections. It was also very important to take into account the low energy particles cascading in nuclei. We have found only 2 papers with experimental data on antideuteron-nucleus interactions [31, 32]. The data were obtained with liquid hydrogen bubble chamber of LHE JINR irradiated by antideuterons with momentum of 12.2 GeV/c. The statistics of the data are small, about 2 – 3 thousand events.

We show the experimental data for the $\bar{d}d$ interactions [31] and our calculations in Fig. 8. As seen, very promising results are obtained for the interactions. In the left figure, we present p_T^2 distributions of π^- mesons and antineutrons. The π^- meson data and calculations are given by blue points and blue lines. The antineutron data and corresponding calculations are given by red points and red lines. As seen, a good agreement between the data and calculations by FTF+PRECO is reached. In the middle figure, we show p_T^2 distributions of positive and negative charged particles. We also have obtained a good description of the data (red and blue points) by FTF+PRECO (red and blue lines). In the right figure, we give the data on rapidity distributions of π^- mesons (blue points) and π^+ mesons (red points). Blue and red lines are correspondingly FTF+PRECO calculations. We have not used any additional tuning of the FTF model for the description of these data. Cross sections of $\bar{d}d$ interactions were taken from previous calculations. We have not considered a possible absorption of mesons in the liquid hydrogen chamber which can be responsible for the small difference between the data and the model calculations in the central region.

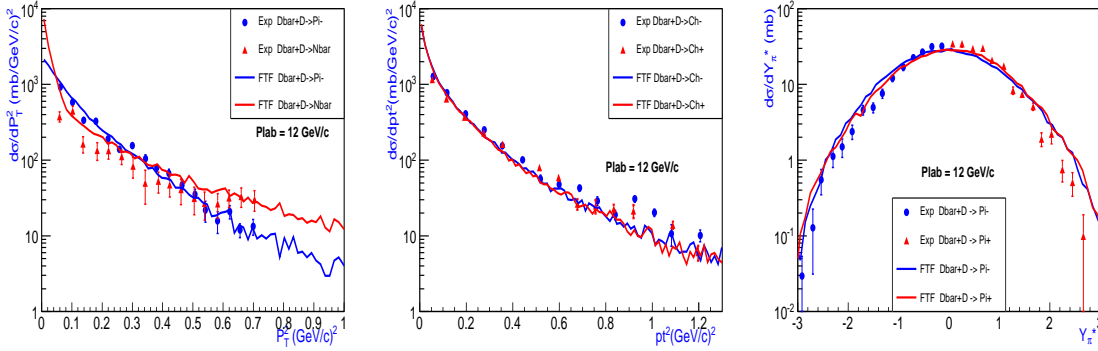


Figure 8: Distributions of particles on kinematical variables in antideuteron-deuteron interactions at 12.2 GeV/c. Points are experimental data [31]. Lines are our calculations.

In the next experiment [32], a tantalum plate disposed in the chamber was irradiated by a beam of antideuterons with momentum of 12.2 GeV/c. The multiplicity distribution of charged particles produced in the interactions are shown in the Fig. 9 (left) in a comparison with calculations by FTF+PRECO (blue lines) and FTF+Binary (red lines). As seen, the models describes the data rather well. Another situation takes place with multiplicity distributions of protons produced in the $\bar{d}Ta$ interactions. Both combinations of the models cannot describe the data quite well. According to Ref. [32], only protons with momenta larger than 300 MeV/c were observed. The slow protons were absorbed by the Ta plate. We took into account this restriction. Additional to this, we assumed that π -mesons with momenta less than 100 MeV/c were also absorbed by the plate. These did not help too much. Probably, the difference between the calculations and the data is connected with beam background. According to Ref. [32], the beam had 40% admixture of π^- mesons, which we

did not considered. Maybe other experimental conditions have to be taken into account. We are going to study these data more carefully in the future.

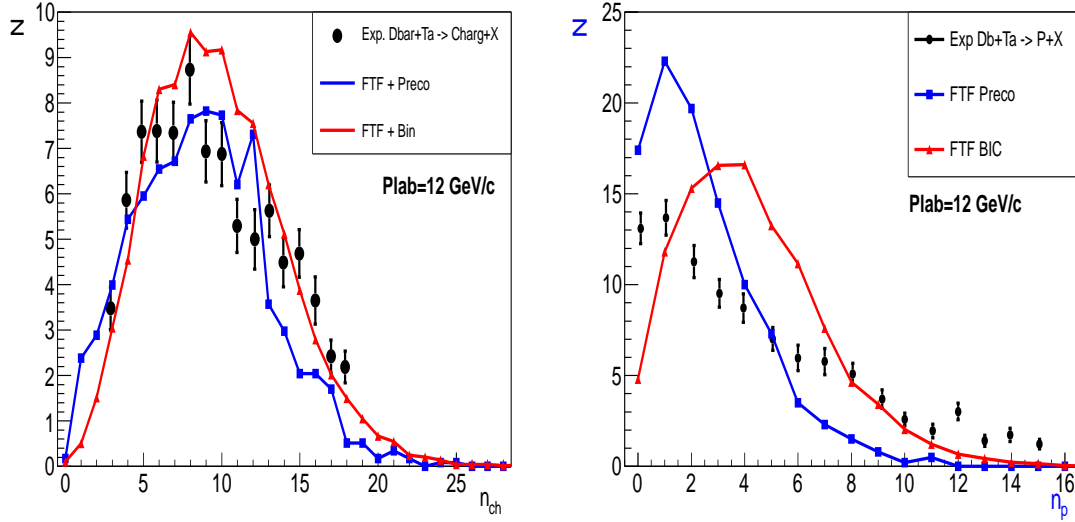


Figure 9: Multiplicity distributions of charged particles and protons in antideuteron-deuteron interactions at 12.2 GeV/c. Points are experimental data [32]. Lines are our calculations.

We can conclude that FTF model in Geant4 reproduces general features of antinucleus-nucleus interactions.

Conclusion

A model of antibaryon-nucleon, antibaryon-nucleus and antinucleus-nucleus interactions combined many phenomenological approaches is proposed. The model is implemented in Geant4 toolkit starting from the version 9.6. It includes:

- Estimation of antibaryon-nucleon process's cross sections;
- Calculation of antibaryon-nucleus and antinucleus-nucleus interaction cross sections in the Glauber approach;
- Finite energy corrections to the AGK cutting rules;
- Reggeon theory inspired model of nuclear destruction (RTIM) at high energies;
- Formation time for low energy secondary particles and their cascading;
- Nuclear residual de-excitation models of Geant4.

All of these allow one to describe main properties of the interactions.

The authors are thankful to the Geant4 hadronic working group for stimulating discussions and interest to the work.

References

- [1] S. Agostinelli (GEANT4 Collaboration), Nucl. Instrum. Methods, **A506**, 250 (2003);
J. Allison (GEANT4 Collaboration), IEEE Trans. Nucl. Sci., **53**, 270 (2006).
- [2] A. Capella, U. Sukhatme, C-I Tan, J. Tran Thanh Van, Phys. Rept., **236**, 225 (1994).
A.B. Kaidalov and K.A. Ter-Martirosian, Phys. Lett. **B117**, 247 (1982).
- [3] R.J.Glauber, In: "Lectures in Theoretical Physics", Ed. W.E.Brittin et al., v. **1**, Interscience Publishers, N.Y., 1959.;
R.J.Glauber, Proc. of the 2nd Int. Conf. on High Energy Physics and Nuclear structure, (Rehovoth, 1967) Ed. G.A.Alexander, North-Holland, Amsterdam, 1967;
- [4] V.Franco, Phys. Rev., **175**, 1376 (1968);
- [5] W.Czyz and L.C.Maximon, Ann. of Phys. (N.Y.), **52**, 59 (1969).
- [6] V.V. Uzhinsky and A.S. Galoyan, arXiv:0212369 [hep-ph].
- [7] A.Galoian and V.Uzhinsky, AIP Conf.Proc., **796**, 79 (2005).
- [8] V. Flaminio, W.G. Moorhead, D.R.O. Morrison and N. Rivoire. Compilation of cross-sections: p and \bar{p} induced reactions, CERN-HERA 84-01, 1984.
- [9] V. Uzhinsky, Proc. Intern. Conf. on Calor. for the High Energy Frontier (CHEF 2013), C13-04-22.4, p.260.
<http://geant4.cern.ch/support/userdocuments.shtml/PhysicsReferenceManual.pdf>
- [10] V. Franco and R.J. Glauber, Phys. Rev., **142**, 1195 (1966).
- [11] O.D. Dalkarov and V.A. Karmanov, Nucl. Phys., **A445**, 579 (1985).
- [12] V. Uzhinsky, J. Apostolakis, A. Galoyan et al., Phys. Lett., **B705**, 235 (2011).
- [13] W. Broniowski, M. Rybczynski and P. Bozek, Comp. Phys. Commun., **180**, 69 (2009).
- [14] V.V. Uzhinsky and S. Yu. Shmakov, Phys. Atom. Nucl., **57**, 1459 (1994) (Yad. Fiz., **57**, 1532 (1994)).
- [15] L.S. Azhgirei et al., Nucl. Phys., **A305**, 397 (1978).
- [16] S. Shmakov, V. Uzhinsky and A. Zadorozhny, Comp. Phys. Comm., **54**, 125 (1989).
- [17] J.V. Allaby et al., Yad. Fiz., **12**, 538 (1970); R.J. Abrams et al., Phys. Rev., **D4**, 3235 (1971); S.P. Denisov et al., Nucl. Phys., **B61**, 62 (1973); A.S. Carroll et al., Phys. Lett., **80B**, 319 (1979); A.M. Schiz, FERMILAB-THESIS-1979-17, UMI-80-12109 (1979); Yu.P. Gorin et al., Yad. Fiz., **18**, 336 (1973); R. Bailey et al., Zeit. fur Phys., **C29**, 1 (1985); K.Nakamura et al., Phys. Rev. Lett., **52**, 731 (1984); V. Ashford et al., Phys. Rev., **C31**, 663 (1985); G. Bendiscioli, A. Rotondi, and A. Zenoni, Nuov. Cim., **104A**, 59 (1991); V.F. Kuzichev, Yu.B. Lepikhin, and V.A. Smirnitsky, Nucl. Phys., **A576**, 581 (1994).
- [18] S.P. Denisov et al., Nucl. Phys., **B31**, 253 (1971).
- [19] V.A. Abramovsky, V.N. Gribov and O.V. Kancheli, Sov. J. Nucl. Phys., **18**, 308 (1974) (Yad. Fiz., **18**, 595 (1973)).
- [20] A. Galoyan and V.Uzhinsky, Hyperfine Interactions, **215**, 69 (2013); arXiv:1208.3614 [nucl-th].
- [21] K.G. Boreskov, A.B. Kaidalov, S.M. Kiselev and N.Ya. Smorodinskaya, Sov. J. Nucl. Phys., **53**, 356 (1991) (Yad. Fiz., **53**, 569 (1991)).

- [22] K. Abdel-Waged and V.V. Uzhinsky, Phys. Atom. Nucl., **60**, 828 (1997) (Yad. Fiz., **60**, 925 (1997)); Kh. Abdel-Waged and V.V. Uzhinsky, J. Phys., **G24**, 1723 (1997).
- [23] G. Folger, V.N. Ivanchenko and J.P. Wellisch, Eur. Phys. J., **A21**, 407 (2004).
<http://geant4.web.cern.ch/geant4/UserDocumentation/UsersGuides/PhysicsReferenceManual/fo/PhysicsReferenceManual.pdf>
- [24] S. Furihata, NIM, **B171**, 251 (2000).
- [25] J. Rielberger, Nucl. Phys. (Proc Suppl), **B8**, 288 (1989); P.L.McGaughey et al., Phys. Rev. Lett., **56**, 2156 (1986); H.J. Bersch et al., Zeit. fur Phys., **A292**, 197 (1979).
- [26] Ye.S. Golubeva et al., Nucl. Phys., **A483**, 539 (1988); E.S. Golubeva, A.S. Ilinov, B.V. Krippa and I.A. Pshenichnov, Nucl. Phys., **A537**, 393 (1992); I.A. Pshenichnov, A.S. Ilinov, E.S. Golubeva and D. Polster, Phys. Rev., **C52**, 947 (1995).
- [27] A.B. Larionov, I.A. Pshenichnov, I.N. Mishustin and W. Greiner, Phys. Rev., **C80**, 021601 (2009); A.B. Larionov, T. Gaitanos and U. Mosel, Phys. Rev., **C85**, 024614 (2012); A.B. Larionov, arXiv:1410.7625 [nucl-th].
- [28] T. von Egidy et al., Eur. Phys. J., **A8**, 197 (2000);
- [29] R. Bailey et al., Zeit. fur Phys., **C29**, 1 (1985).
- [30] C. De Marzo et al., Phys. Rev., **D26**, 1019 (1982).
- [31] B.V. Batyunya et. al, JINR Preprint P1-87-849
- [32] V.F. Andreev et. al, Nuov. Cim., **103A**, 1163 (1989).